Growth of two-dimensional Au patches in graphene pores: a density-functional study

Saku Antikainen

UNIVERSITY OF JYVÄSKYLÄ

Alkusanat

Tämä Pro gradu -tutkielma koostuu suomenkielisestä johdanto-osuudesta ja varsinaisesta julkaistavaksi lähetetystä artikkelista. Johdannossa käydään läpi menetelmiä, joita gradussa käytettiin.

Työn tavoitteena oli simuloida kaksiulotteisen kultasaarekkeen kasvua grafeenin reunalle. Kasvuprosessi on jaettu neljään vaiheeseen: i) kulta-atomit liikkuvat grafeenikerroksen päällä, ii) kulta-atomit saapuvat grafeeni-kulta rajapinnalle, iii) kulta-atomit liikkuvat 2D-kultatason päällä, ja iv) kulta-atomit saapuvat 2D-kultatason reunalle. Päätarkoituksena oli tutkia kuinka helposti kulta-atomit liikkuvat grafeenitason reunalle, ja asettuvatko kulta-atomit kaksiulotteisesti samaan tasoon grafeenin kanssa. Tämän johdannon tarkoituksena on antaa yleiskuva laskuista ja laskuissa käytetyistä metodeista.

1 Johdanto

Yleisesti laskut etenivät jokaisessa vaiheessa samalla tavalla: kulta-atomi asetettiin eri adsorptiopaikkoihin joko grafeeni- tai kultatason päälle tai reunalle, minkä jälkeen systeemin annettiin relaksoitua. Näin saatiin laskettua adsorptioenergiat yhtälöstä

$$E_{ads} = E_{2D} + E_{Au\ atom} - E_{relax},\tag{1}$$

missä E_{2D} on systeemin energia ilman lisättyä kulta-atomia, $E_{Au\ atom}$ on vapaan kulta-atomin energia, ja E_{relax} on relaksoidun systeemin energia. Tämän jälkeen tutkimuksen kohteena oli kulta-atomin diffundoituminen adsorptiopaikkojen välillä käyttäen Nudged Elastic Band -metodia [1]. Poikkeuksen muodosti vaihe 2 (grafeeni-kulta rajapinta), jossa kulta-atomeita lisättiin useampi kappale yksi kerrallaan grafeenin reunalle.

Kaikki energiat on laskettu käyttäen tiheysfunktionaaliteoriaa (density-functional theory, DFT), jonka perusteet esitellään kappaleessa 1.1. Oleellinen osa tiheysfunktionaaliteoriaa on ns. vaihto- ja korrelaatiofunktionaali, jonka approksimointiin on kehitetty useita metodeja, esimerkiksi LDA-, GGA-, ja van der Waals -funktionaalit. Tässä työssä on käytetty Perdew-Burke-Ernzerhofin PBE-funktionaalia [5], joka kuuluu GGA-funktionaalien joukkoon. Laskut tehtiin GPAW-ohjelmistolla [2,3], joka perustuu projector-augmented wave -metodiin (PAW [4]). PAW käyttää ns. pseudo-aaltofunktioita oikeiden aaltofunktioiden sijaan; tämä yksinkertaistaa laskuja huomattavasti. Laskuissa käytettiin LCAO-moodia, missä aaltofunktiot esitetään atomiorbitaalien lineraarikombinaatioina.

1.1 Tiheysfunktionaaliteoria

1.1.1 Hohenberg-Kohn teoreemat

Tiheysfunktionaaliteoria (DFT) tarjoaa keinon ratkaista monen kappaleen Schrödingerin yhtälö

$$\hat{H}\Psi = (\hat{T} + \hat{V} + \hat{U}) = E\Psi,\tag{2}$$

missä $\hat{H}$ on systeemin Hamiltonin operaattori, $\hat{T}$ kuvaa elektronien liike-energiaa, $\hat{V}$ elektroni-elektroni vuorovaikutusta, ja $\hat{U}$ elektroni-ydin vuorovaikutusta. Oletuksena on Born-Oppenheimer-approksimaatio: ytimien kineettinen energia jätetään huomiotta, ja ytimien oletetaan olevan paikallaan elektroneiden kannalta, johtuen ytimien huomattavasti suuremmasta massasta.

Tiheysfunktionaaliteorian perustana on kaksi Hohenberg-Kohn teoreemaa [7]. Ensimmäisen mukaan ulkoinen potentiaali $V_{ext}(\vec{r})$ voidaan esittää elektronitiheyden funktionaalina. Toisen teoreeman mukaan systeemin perustilan energia E saadaan minimoimalla funktionaali $E[n]$; tiheys joka minimoi tämän energian on täsmälleen systeemin perustilan tiheys. Määrittämällä Hohenberg-Kohn funktionaali

$$F_{HK}[n] = T[n] + E_{ee}[n]\tag{3}$$

energia voidaan kirjoittaa

$$E_{HK}[n] = T[n] + E_{ee}[n] + E_{ext}[n]$$
$$= F_{HK}[n] + \int V_{ext}(\vec{r})n(\vec{r})\mathrm{d}\vec{r}, \tag{4}$$

missä ydin-elektroni vuorovaikutuksesta johtuva energia voidaan kirjoittaa muodossa $E_{ext}[n] = \int V_{ext}(\vec{r})n(\vec{r})\mathrm{d}\vec{r}$. Hohenberg-Kohn teoreemat eivät tarjoa konkreettista keinoa laskea tiheyttä tai energiaa, mutta tästä jatkamaan kehitettiin Kohn-Sham formalismi. [6]

1.1.2 Kohn-Sham formalismi

Kohn-Sham formalismissa [8] oikea vuorovaikuttava systeemi korvataan uudella vuorovaikuttamattomalla referenssisysteemillä, jonka perustilan tiheys on sama kuin oikealla systeemillä, ja elektronien katsotaan liikkuvan ns. Kohn-Sham potentiaalissa $V_{KS}(\vec{r})$. Yhtälön (3) E_{ee} voidaan jakaa kahteen osaan: tunnettuun klassiseen Coulombin energiaan $E_H[n]$ (Hartree-energia) ja tuntemattomaan ei-klassiseen osaan $E_{ncl}[n]$:

$$E_{ee} = E_H[n] + E_{ncl}[n] = \frac{1}{2}\iint \frac{n(\vec{r_1})n(\vec{r_2})}{r_{12}}\mathrm{d}\vec{r_1}\mathrm{d}\vec{r_2} + E_{ncl}[n]. \tag{5}$$

Vuorovaikuttamattoman systeemin kineettinen energia tunnetaan, ja se voidaan ilmoittaa yksittäisten elektroneiden aaltofunktioiden (spin-orbitaalien) ψ_i avulla:

$$T_S = -\frac{1}{2}\sum_i^N \left\langle \psi_i \left| \nabla^2 \right| \psi_i \right\rangle. \tag{6}$$

Näiden spin-orbitaalien neliöt summautuvat oikean systeemin perustilan tiheydeksi, ts.

$$n_0(\vec{r}) = \sum_i^N \sum_s |\psi_i(\vec{r}, s)|^2. \tag{7}$$

Nyt yhtälöstä (3) saadaan

$$F[n] = T_S[n] + (T[n] - T_S[n]) + E_H[n] + E_{ncl}[n]$$
$$= T_S[n] + E_H[n] + E_{xc}[n], \tag{8}$$

missä termiin $E_{xc}[n]$ on koottu kaikki tuntematon:

$$E_{xc}[n] = (T[n] - T_S[n]) + E_{ncl}[n] \tag{9}$$

Funktionaalia $E_{xc}[n]$ sanotaan vaihto- ja korrelaatiofunktionaaliksi (xc-funktionaali). [6]

1.1.3 Kohn-Sham yhtälöt

Systeemin energia on nyt

$$E[n] = T_S[n] + E_H[n] + E_{xc}[n] + E_{ext}[n]. \tag{10}$$

Käyttämällä variaatioperiaatetta, ts. minimoimalla yhtälö (10) tiheyden suhteen voidaan johtaa ns. Kohn-Sham yhtälöt:

$$\left(-\frac{1}{2}\nabla^2 + V_{KS}(\vec{r}) \right) \psi_i = \varepsilon_i \psi_i, \tag{11}$$

missä Kohn-Sham potentiaali $V_{KS}(\vec{r})$ on

$$\begin{aligned} V_{KS}(\vec{r}) &= V_{ext}(\vec{r}) + \frac{\delta E_H}{\delta n} + \frac{\delta E_{xc}}{\delta n} \\ &= V_{ext}(\vec{r}) + V_H(\vec{r}) + V_{xc}(\vec{r}). \end{aligned} \tag{12}$$

Tiheysfunktionaaliteorian keskipisteessä on vaihto- ja korrelaatiofunktionaalin $E_{xc}[n]$ ja samalla potentiaalin V_{xc} approksimointi; sen avulla saadaan ratkaistua orbitaalit Kohn-Sham yhtälöistä ja orbitaalien avulla perustilan tiheys yhtälöstä (7). [6]

1.2 XC-funktionaalin approksimointi

Käytännössä approksimoinnissa xc-funktionaali jaetaan vaihto- ja korrelaatioosiin

$$E_{xc} = E_x + E_c, \tag{13}$$

joita approksimoidaan erikseen. Yleisiä xc-funktionaalin approksimaatioita ovat paikallistiheysapproksimaatio (local-density approximation, LDA), yleistetty gradienttiapproksimaatio (generalized gradient approximation, GGA), hybridifunktionaalit, ja van der Waals -funktionaalit. LDA on näistä yksinkertaisin: tiheydeksi oletetaan homogeenisen elektronikaasun tiheys. Tämä malli toimii hyvin esimerkiksi yksinkertaisilla metalleilla, mutta pettää usein monimutkaisemmilla systeemeillä, joilla tiheys vaihtelee voimakkaasti. GGA-funktionaaleissa käytetään tiheyden lisäksi myös tiheyden gradienttia $\nabla n(\vec{r})$; tällöin myös ympäristön muutokset tiheydessä otetaan huomioon kussakin pisteessä. Yleisiä GGA-funktionaaleja ovat esimerkiksi BLYP [9, 10] ja tässäkin työssä käytetty PBE.

LDA- ja GGA-funktionaalit ovat lokaaleja funktionaaleja, ts. epälokaalit van der Waals -vuorovaikutukset jäävät kokonaan huomiotta. Tätä varten on kehitetty ns. van der Waals -funktionaaleja, joiden tavoitteena on ottaa myös vdW-vuorovaikutus huomioon. Yleisiä vdW-funktionaaleja ovat esimerkiksi VdW-DF [11], VdW-DF2 [12], Grimme DFT-D [13], ja VV10 [14]. Nämä funktionaalit tuottavat tarkempia tuloksia monille materiaaleille, joissa vdW-vuorovaikutus on vahva verrattuna muihin sidosvoimiin. Usein kuitenkin vdW-voimat ovat verrattain pieniä esimerkiksi kovalenttisesti sitoutuneissa materiaaleissa, joten vdW-funktionaalien käyttö ei ole aina välttämättömyys.

1.3 PBE

Perdew-Burke-Ernzerhofin PBE-funktionaalissa [5] vaihto-osa E_{x} voidaan esittää muodossa

$$E_{\mathrm{x}}^{\mathrm{PBE}} = \int \mathrm{d}^3 r n(r) \epsilon_{\mathrm{x}}^{\mathrm{unif}}(n) F_{\mathrm{x}}(s), \tag{14}$$

missä $n(r)$ on tiheys, $\epsilon_{\mathrm{x}}^{\mathrm{unif}} = -3ek_{\mathrm{F}}/4\pi$ on homogeenisen elektronikaasun energiatiheyden vaihto-osa, $k_{\mathrm{F}} = [3\pi^2 n(r)]^{1/3}$ on Fermin aaltovektori. PBE:ssä $F_{\mathrm{x}}(s)$ on määritelty

$$F_{\mathrm{x}}(s) = 1 + \kappa - \frac{\kappa}{1 + \mu s^2/\kappa}, \tag{15}$$

missä $\kappa = 0.804$, $\mu = 0.21951$, ja $s = |\nabla n|/2k_{\mathrm{F}}n$ on dimensioton tiheysgradientti.

PBE-funktionaalin korrelaatio-osa on

$$E_{\mathrm{c}}^{\mathrm{PBE}} = \int \mathrm{d}^3 r n(r) [\epsilon_{\mathrm{c}}^{\mathrm{unif}}(r_s, \zeta) + H(r_s, \zeta, t)], \tag{16}$$

missä $r_s = [(4\pi/3)n]^{1/3}$ on lokaali Seitzin säde, $\zeta = (n_\uparrow - n_\downarrow)/n$ on suhteellinen spin-polarisaatio, $t = |\nabla n|/2\phi k_s n$ on dimensioton tiheysgradientti. Tiheysgradientissa esiintyvä $\phi(\zeta) = [(1+\zeta)^{2/3} + (1-\zeta)^{2/3}]/2$ on spinin skaalauskerroin ja $k_s = \sqrt{4k_F/\pi a_0}$, missä $a_0 = \hbar^2/me^2$. PBE:ssä funktiolle H on johdettu muoto

$$H = (e^2/a_0)\gamma\phi^3 \ln\left(1 + \frac{\beta}{\gamma} t^2 \left[\frac{1 + At^2}{1 + At^2 + A^2 t^4}\right]\right), \tag{17}$$

missä $\gamma = 0.031091$, $\beta = 0.066725$, ja $A = (\beta/\gamma)[\exp\{-\epsilon_{\mathrm{c}}^{\mathrm{unif}}/(\gamma\phi^3 e^2/a_0)\} - 1]^{-1}$. PBE:ssä ei ole empirisiä parametreja; kaikki parametrit on johdettu asettamalla ehtoja esimerkiksi tiheysgradienteille niiden lähestyessä nollaa tai ääretöntä.

1.4 Nudged Elastic Band -metodi

Nudged Elastic Band -metodin (NEB [1]) tavoitteena on löytää minimienergiapolku (MEP) prosessille, jonka alku- ja lopputila on tiedossa. Alku- ja lopputilan välille luodaan joukko kopioita (ts. kuvia) systeemistä muodostaen alkuarvaus polulle. Polun jatkuvuuden varmistamiseksi vierekkäisten kuvien välille lisätään jousivuorovaikutus. Systeemit optimoidaan minimoimalla vaikuttava voima kuhunkin kuvaan, ja lopputuloksena saadaan minimienergiapolku (Kuva 1). Optimointiprosessissa lisätystä jousivoimasta lasketaan vain polun kanssa yhdensuuntainen komponentti $F_{S\parallel}$ ja todellisesta voimasta polkua vastaan kohtisuora komponentti $F_\perp$, ts. NEB-voima on

$$F_{\mathrm{NEB}} = F_{S\parallel} + F_\perp. \tag{18}$$

Tämä varmistaa, etteivät jousivoimat vaikuta MEP-konvergenssiin, eikä todellinen voima kuvien jaotteluun.
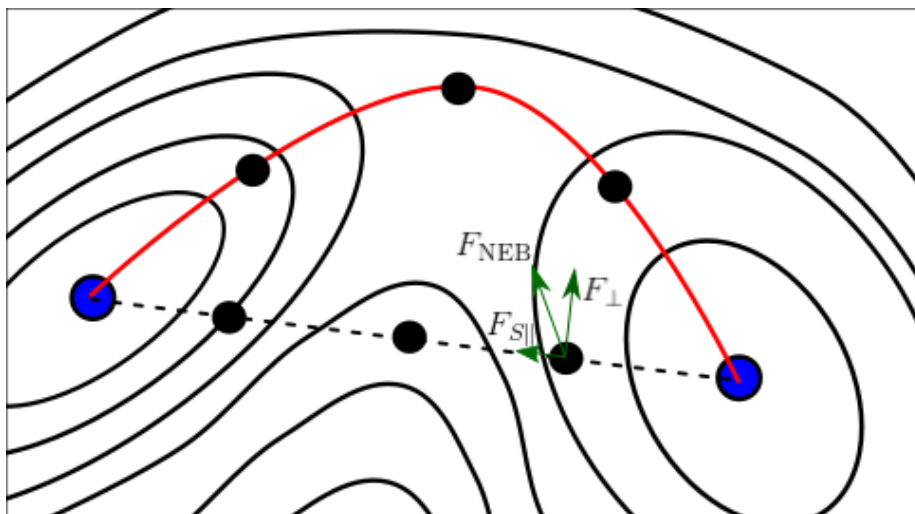
Kuva 1: Nudged Elastic Band -metodia havainnollistava kuva. Katkoviivalla merkitty polku on alkuarvaus minimienergiapolulle. Minimienergiapolku on punaisella merkitty polku. Tässä tapauksessa on käytetty kolmea kuvaa (mustat ympyrät) alku- ja lopputilan (siniset ympyrät) välillä. Alkupolusta päädytään lopulta minimienergiapolkuun minimoimalla vaikuttava voima kuhunkin kuvaan usean iteraation jälkeen.

Tässä työssä käytettiin kolmea kuvaa alku- ja lopputilan välillä; reaktiopolut olivat melko yksinkertaisia, joten tämä kuvien määrä oli riittävä. Alku- ja lopputilat olivat vierekkäiset adsorptiopaikat joko grafeeni- ja kultatasojen päällä tai reunalla. Toistamalla laskut kaikkien adsorptiopaikkojen välillä saatiin lopulta potentiaalienergiapinta, joka kuvaa kulta-atomin reittiä tason päältä reunalle. Useissa reunalaskuissa NEB-metodia ei kuitenkaan tarvittu, koska tason päällä lähellä reunaa ei löytynyt stabiilia adsorptiopaikkaa, vaan kulta-atomi siirtyi optimoinnissa suoraan reunalle.

Viitteet

[1] G. Henkelman and H. Jonsson, *Improved Tangent Estimate in the NEB method for Finding Minimum Energy Paths and Saddle Points*, J. Chem. Phys. 113, 9978 (2000)

[2] J. J. Mortensen, L. B. Hansen , and K. W. Jacobsen, *Real-space grid implementation of the projector augmented wave method*, Physical Review B, Vol. 71, 035109, 2005

[3] J. Enkovaara, C. Rostgaard, J. J. Mortensen et al. *Electronic structure calculations with GPAW: a real-space implementation of the projector augmented-wave method*, J. Phys.: Condens. Matter 22, 253202 (2010)

[4] P. E. Blöchl, *Projector augmented-wave method*, Physical Review B, Vol. 50, 17953, 1994

[5] J. P. Perdew, K. Burke, and M. Ernzerhof, *Generalized Gradient Approximation Made Simple*, Phys. Rev. Lett. 77, 3865 (1996)

[6] Wolfram Koch, Max C. Holthausen, *A Chemist's Guide to Density Functional Theory, Second Edition*, Wiley-VCH, 2001, ISBN 3-527-30422-3

[7] P. Hohenberg, W. Kohn, *Inhomogeneous Electron Gas*, Phys. Rev. 136:B864-871, 1964.

[8] W. Kohn, L. J. Sham, *Self-Consistent Equations Including Exchange and Correlation Effects*, Phys. Rev. 140:A1133-1138, 1965.

[9] A. D. Becke, *Density-functional exchange-energy approximation with correct asymptotic behavior*, Phys. Rev. A 38:3098, 1988.

[10] Chengteh Lee, Weitao Yang, Robert G. Parr, *Development of the Colle-Salvetti correlation-energy formula into a functional of the electron density*, Phys. Rev. B 37:785, 1988.

[11] M. Dion et al., *Van der Waals Density Functional for General Geometries* Phys. Rev. Lett. 92:246401, 2004.

[12] K. Lee et al., *Higher-accuracy van der Waals density functional*, Phys. Rev. B 82:081101, 2010.

[13] S. Grimme, *Accurate description of van der Waals complexes by density functional theory including empirical corrections*, J. Chem. Phys. 25:1463, 2004.

[14] O. A. Vydrov, T. Van Voorhis, *Nonlocal van der Waals density functional: The simpler the better*, J. Chem. Phys. 133:244103, 2010.

Growth of two-dimensional Au patches in graphene pores: a density-functional study

Saku Antikainen[1] and Pekka Koskinen[1]

[1] *NanoScience Center, Department of Physics, University of Jyvaskyla, 40014 Jyvaskyla, Finland*

Inspired by recent studies of various two-dimensional (2D) metals such as Au, Fe and Ag, we study the growth of two-dimensional gold patches in graphene pores by density-functional theory. We find that at room temperature gold atoms move readily on top of both graphene and two-dimensional gold with energy barriers less than 0.5 eV. Our calculations show that gold atoms have energy barriers neither for moving from the top of graphene to its edge nor for moving from the top of 2D gold to its edge. The energy barriers are absent even at the interface of 2D gold and graphene, so that the gold atoms move effortlessly across the interface. We hope our demonstration for the propensity of diffusing gold atoms to grow 2D gold patches in graphene pores will inspire the fabrication of these patches experimentally.

I. INTRODUCTION

The great success with graphene has sparked much additional interest to other possible two-dimensional (2D) materials. The dimensionality can change the properties of the material greatly, of which graphene is a prime example: it has extremely high carrier mobility and thermal conductivity, and it demonstrates the Quantum Hall effect.[1,2] Another example is the transition-metal dichalcogenide MoS_2: bulk MoS_2 is an indirect bandgap semiconductor, while a monolayer MoS_2 becomes a direct gap semiconductor.[3,4] Both graphite and bulk MoS_2 consist of covalently bound layers that are held together by the weak van der Waals (vdW) interactions. Bulk metals have no such layered structure, and thus the fabrication of two-dimensional metallic structures is more problematic. However, the recent interest in 2D metals has generated a number of studies to inspect the possibility of their existence.

For example, the simulations of 2D metals have shown promising results about their stability. For gold Yang et al. have predicted a stable, two-dimensional lattice structure with hexagonal symmetry.[5] In addition, bond strength was found to increase greatly when going from bulk 3D Au to 2D Au, analogously to the case of 3D diamond and 2D graphene. Similar predictions were made for 2D silver, which was also found to prefer a hexagonal lattice structure.[1] In addition to static properties, Koskinen and Korhonen have predicted the existence of a liquid phase of a free-standing, atomically thin 2D Au layer suspended in graphene pores.[6] However, a free-standing two-dimensional layer of gold is yet to be produced experimentally. Zhao et al. have managed to create a single-atom-thick iron layer suspended in graphene pores[7]; this idea could likewise be applied to other metals. Shao et al. suggest with their simulations that a square lattice monolayer Fe is energetically unstable, and that the experimentally observed Fe monolayers would instead be made of a mixture of Fe and C.[8] The possibility of a combination of carbon and metal is certainly worth investigating in further studies of 2D metals.

In any case, recent studies indicate that gold in particular is an interesting candidate for a 2D metal. In nanoscale, gold has been found to behave very differently from the inert bulk gold. For example, small gold clusters of up to 20 atoms have been shown to exhibit catalytic activity with the combustion of CO.[9] It is known that small gold cluster anions of up to 12 or even 13 atoms have two-dimensional ground states.[10,11] This exceptional planar stability is attributed to the relativistic effects on gold. The studies of 2D Au have been promising, but creating a free-standing 2D monolayer of gold is experimentally problematic. Yet it has been shown that a gold atom interacts strongly with a graphene edge.[12] These properties of gold, combined with the success of producing a Fe monolayer suspended in graphene pores, give faith that two-dimensional structures could be synthesized with gold and perhaps even with other metals.

Here we have simulated the growth of a 2D gold patch at the edge of graphene using density-functional theory (DFT) in order to study how the Au atoms behave at the graphene edge and how the 2D gold patch grows. We performed DFT calculations to investigate the behavior of gold atoms at different stages of the growth process. We analyze the growth process in four stages: i) originating from some source of atomic gold, gold atoms move on top of a graphene sheet, ii) a gold patch begins to form at the edge of the graphene, iii) gold atoms move on top of the gold patch, and iv) the gold atoms move from the top of the gold patch to the edge of the gold patch, thereby growing the patch. We studied the adsorption of gold at different adsorption sites on top of the graphene and 2D gold sheets, as well as at the edge of the sheets. In addition, we determined the potential energy surfaces (PES) for the movement of gold atoms between various adsorption sites. These potential energy landscapes indicate clearly that gold atoms prefer to move quickly from the top of graphene across the graphene-gold interface and to the edge of the 2D gold patch.

II. METHODS

Our goal was to model the growth of a gold patch at the edge of a graphene pore. More precisely, we modeled gold atoms moving on top of graphene towards the edge so that when they met the edge a gold patch began to form. Hence the overall process could be broken into four stages, as sketched in Figure 1. First, we used a 2D graphene sheet with a single gold atom at various adsorption sites. Second, to model the growth of graphene-2D metal interface we used graphene nanoribbon with varying number of gold atoms at the edge. We used both a zig-zag-edged graphene nanoribbon (ZGNR) and an armchair-edged graphene nanoribbon (AGNR). Third, we used a 2D gold sheet with a single gold atom at various adsorption sites. And fourth, to model the actual growth of the gold patch we used a one-dimensional
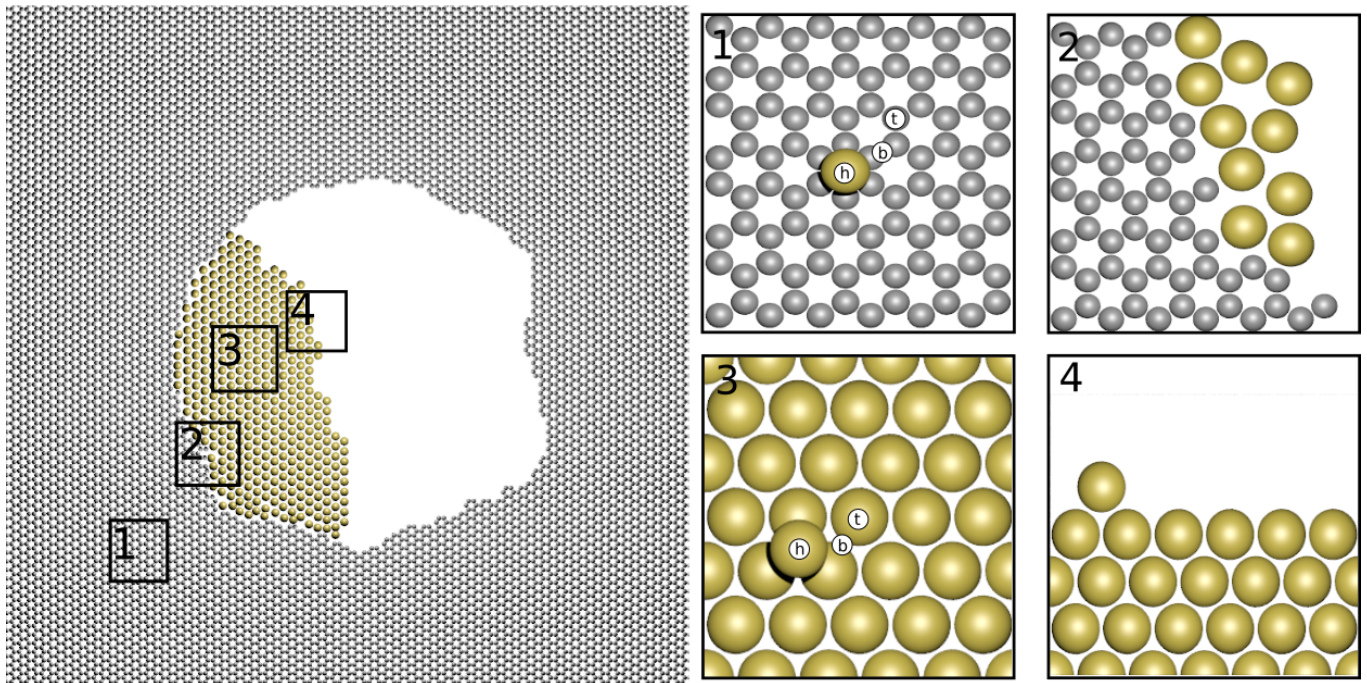
Fig. 1. Overall picture of the growth process. On the left is an infinite 2D graphene sheet with a growing patch of gold in the middle. The growth process is divided into four pieces, labeled 1-4: 1) a 2D periodic graphene sheet with top[t], hollow[h] and bridge[b] adsorption sites, 2) a 1D periodic graphene zigzag-edge and armchair-edge with gold at the edge, 3) a 2D periodic gold patch with top[t], hollow[h] and bridge[b] adsorption sites, and 4) a 1D periodic gold edge.

gold edge with an additional gold atom at the edge.

The DFT calculations were performed using atomic simulation environment[13] and GPAW[14,15], which is based on the projector-augmented wave method (PAW)[16]. The generalized gradient approximation exchange-correlation functional of Perdew, Burke, and Ernzerhof (PBE)[17] was used throughout the calculations. All calculations were made in local basis mode (LCAO) with double-zeta polarized basis, and some additional calculations in Finite Difference (FD) mode.

For the 2D structures (2D Au and graphene), the convergence of adsorption energy of a single Au atom on the 2D sheet was tested with respect to unit cell size and k-point sampling. The adsorption energy was calculated according to equation

$$E_{\mathrm{ads}} = E_{\mathrm{2D}} + E_{\mathrm{Au\ atom}} - E_{\mathrm{relax}}, \qquad (1)$$

where E_{2D} is the energy of the 2D sheet without the adsorbate, $E_{\mathrm{Au\ atom}}$ is the energy of a free Au atom and E_{relax} is the energy of the relaxed system. To get E_{relax}, the atoms of the 2D sheet were fixed, while the adsorbate was allowed to move until the forces on all atoms were <0.05 eV/Å. The calculations were made with both LCAO- and FD-mode, but we chose LCAO-mode for the rest of the simulations because its accuracy turned out to be sufficient compared to FD-mode. We chose k-point sampling of 3x3x1 for both of the systems; for 2D Au we chose cell size of 4x4 atoms and for graphene 8x4 atoms, as the adsorption energy was found to be sufficiently converged already at these values. We used a lattice constant of 1.42 Å for graphene and 2.76 Å for 2D Au; the 2D Au

had a hexagonal lattice structure.[5] The 2D sheets were periodic in x-y-plane and non-periodic in z-direction with a 6.0 Å vacuum on both sides of the sheet.

The edges of gold and graphene were modeled using 1D periodic systems. The periodicity was in x-direction with 6.0 Å of vacuum in both y- and z-directions. For the 1D structures (1D Au, ZGNR, and AGNR), the convergence of adsorption energy of an Au atom at the edge with respect to the number of rows of Au or C-atoms in the y-direction was investigated. In these convergence calculations the atom positions were kept fixed because we were merely interested in the convergence of the adsorption energy with respect to the electronic structure rather than the relaxation of the atoms. The edge energy of the nanoribbon was obtained from the equation for the total energy of the nanoribbon:

$$E_{\mathrm{total}} = -N \cdot \varepsilon_{\mathrm{2D}} + L_{\mathrm{edge}} \cdot \varepsilon_{\mathrm{edge}}, \qquad (2)$$

where N is number of atoms in the unit cell, $\varepsilon_{\mathrm{2D}}$ is cohesion energy of the infinite 2D sheet, L_{edge} is the total edge length (2 times the cell x-length) and $\varepsilon_{\mathrm{edge}}$ is the edge energy. We chose the number of atoms in a row to be 12 for AGNR and 10 for ZGNR, as this produced nearly equal unit cell sizes and allowed for enough gold atoms to be placed at the edge. Finally, to keep the cell sizes comparable, the unit cell of 1D Au contained four gold atoms in a row.

To study the actual growth of the gold patch, we added Au atoms one by one to the edge and allowed the system to relax between each added atom, using the Broyden-Fletcher-Goldfarb-Shanno (BFGS)[18] algorithm for opti-

mization. For all the systems described above, we calculated the adsorption energy of a gold atom at different sites. In addition, we studied the potential energy surface (PES) of gold atom on the 2D sheets and along the edges. To calculate the potential energy surfaces between various adsorption sites, we used the nudged elastic band -method (NEB)[19] with 3 images between the start and end points. This number of images was sufficient because the reaction paths were fairly simple.

III.   RESULTS

A.   Stage 1: Gold on graphene

We begun to model the growth process by investigating the movements of a single gold atom on top of graphene. This is a good starting point because much is already known of the diffusion of gold on graphene.[20,21] The obtained adsorption energies of a single Au atom at hollow, bridge, and top sites on 2D graphene were calculated with Equation (1). The adsorption energies are very low, with top-site having slightly higher energy (102 meV) than the bridge-site (96 meV) and hollow-site (73 meV). The study of Amft et al.[22] found similar results (top-site 99 meV and bridge-site 81 meV) with the exception of hollow site, where no binding was predicted. Along with PBE, they also tested other functionals to account for the vdW interaction between the Au atom and graphene. While the introduction of vdW forces increased the adsorption energies, the order of the energies remained the same, with the top site being energetically most favorable. With or without accounting for vdW forces, their calculations showed that the likely diffusion path is along the C-C bonds. We note that, although vdW interactions are often important in 2D materials, the usage of PBE is justified because here the main point of interest is the growth process of gold; in any case the diffusion energy barriers are so low that the choice of functional has on little effect on the main results.

We studied the diffusion of Au atom on graphene for three different paths: top-bridge (t-b), bridge-hollow (b-h) and hollow-top (h-t), the results of which can be seen in Fig. 2. No energy barriers were found on any of these separate paths. As the difference of energies of the top and bridge sites is very low (6 meV), it is reasonable to expect a gold atom to move readily on top of graphene from top site to top site along the bridges; the same conclusion was reached in the aforementioned study of Amft et al.[22]

B.   Stage 2: Gold at graphene edge

Next, to investigate the growth of gold patch at graphene edge we constructed zigzag and armchair graphene nanoribbons with 2-7 rows of C-atoms. In the case of AGNR each row contained 12 C-atoms and in the case of ZGNR each row contained 10 C-atoms. The energy per atom was calculated and plotted as a function of rows (Fig. 3a). We fitted the curve of Eq. (2) for 3-8 rows and thus obtained the edge energies, which can be seen in Fig. 3b. In their simulations of graphene
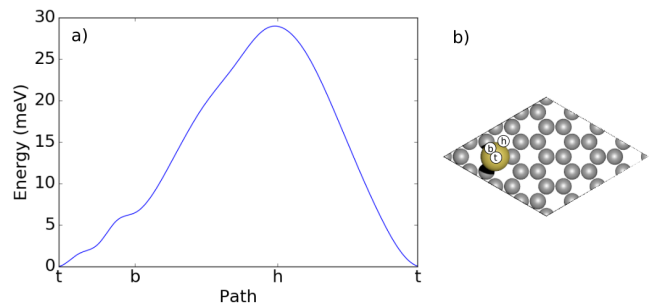

Fig. 2. a) Potential energy surface (PES) of Au atom on top of graphene and b) the unit cell used in calculations, with hollow [h], bridge [b], and top [t] sites marked.
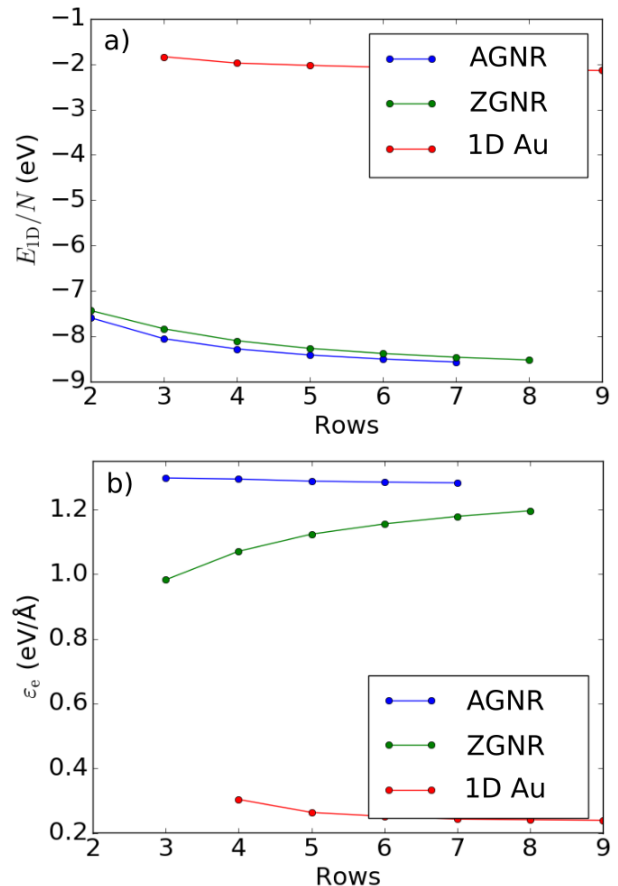

Fig. 3.   a) Energy/atom of 1D gold, AGNR and ZGNR as a function of rows. b) Edge energy of 1D gold, AGNR and ZGNR as a function of rows.

nanoribbons, Koskinen et al. found the edge energies $\varepsilon_{\text{edge}}^{\text{ac}} = 0.98$ eV/Å and $\varepsilon_{\text{edge}}^{\text{zz}} = 1.31$ eV/Å.[23] Our present results are in fair agreement with the earlier numbers, taking into account that we did no optimization at this point and that we fixed the atom positions using constant bond length 1.42 Å of 2D graphene.

Next we added a single gold atom at two different ad-

sorption sites near the edge: at a hollow site on the edge and at a top site on top of the edge. Three rows of C-atoms were used with fixed bottom-row atoms. The systems were allowed to relax and the adsorption energy was calculated. Interestingly, the top sites were not stable at all and during optimization the Au atom moved to a hollow site at the edge. From the edge adsorption energies ($E_{\mathrm{ads}}^{\mathrm{ac}} = 5.62$ eV and $E_{\mathrm{ads}}^{\mathrm{zz}} = 4.61$ eV) we see that the binding is much stronger at the edge than on top of the graphene, which is expected due to available dangling bonds of edge carbon atoms. This is in very much agreement with previous literature results.[12]

Next we studied the movement of the Au atom along the AGNR and ZGNR edges. The results of energy calculations on a path between two edge sites can be seen in Fig. 4. AGNR shows much higher energy barriers (∼1.7 eV) than ZGNR (∼80 meV). This might be attributed to the two carbon atoms the Au atom will have to cross on the AGNR path as opposed to one on the ZGNR path. In other words, in zigzag graphene nanoribbons the dangling bonds are equidistant, whereas in armchair graphene nanoribbons they are separated alternatingly by longer and shorter distances.

Next we gradually begun forming the 2D gold patch to the graphene edge by adding gold atoms one by one. The gold atoms were added to various top sites at the graphene edge (an example is seen in Fig. 4b). A total of 7 atoms were added to AGNR edge and 5 atoms to ZGNR; all optimized systems are shown in Fig. 5. In AGNR, the first three gold atoms settled for the edge sites (such as ones shown in Fig. 4d). The fourth atom also fit in the same row, but the fifth and sixth atoms begun forming a second row of gold. The seventh atom replaced another Au atom in the first row while nudging it further to the second row (Fig. 5h). In other words, the 2D gold patch did not necessarily grow from the edge, but it could also grow from the graphene-gold interface by nudging old gold atoms further back. For comparison, we also studied different 6- and 7-Au atom systems at armchair edge (Fig. 5g and 5i, respectively). Here the six atoms were placed in different starting positions before optimization. This six-atom system (Fig. 5g) was found to have lower energy than the one-atom-at-a-time grown system of Fig. 5f. Again with the addition of the 7th Au atom, we found no energy barrier when moving to the edge. Interestingly, while the unit cells were kept roughly the same size with both AGNR and ZGNR, all 5 atoms fit in the first row with ZGNR. However, this came at the expense of large distortions in z-direction, as shown in Fig. 5o. For ZGNR, we also studied an additional tetragonal geometry, where two gold atoms were bound out of the GNR plane at the edge (Fig. 5l). This system was found to have higher energy than the other two-atom ZGNR system (Fig. 5k) by 2.65 eV. The collapse of 2D structure into 3D is a known possibility at higher temperatures, as demonstrated by Zhao et al. for 2D iron membranes suspended in graphene pores.[7]

C. Stage 3: Gold atom on 2D gold

After investigating the graphene-2D gold interface, we moved on to investigate a gold atom moving on top of 2D gold sheet. The adsorpion energies were obtained for
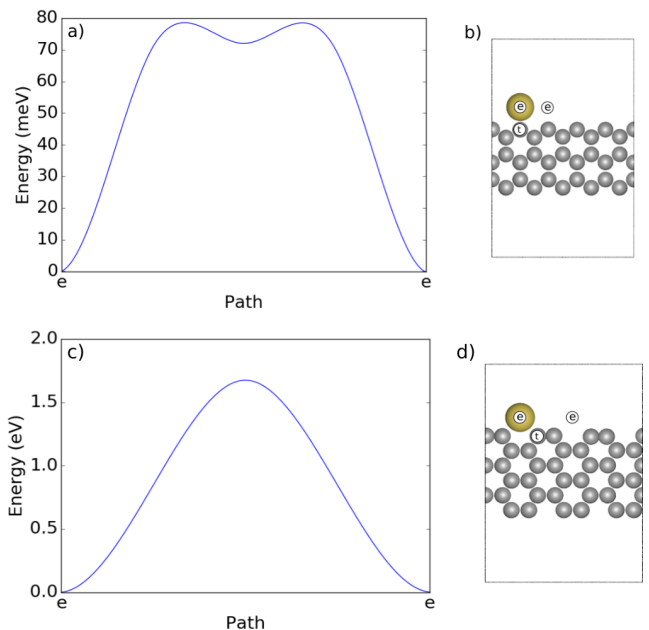

Fig. 4. a) PES of Au atom moving along ZGNR edge, b) the unit cell used in ZGNR calculations, with top [t] and edge [e] sites marked, c) PES of Au atom moving along AGNR edge, and d) the unit cell used in AGNR calculations, with top [t] and edge [e] sites marked.

an Au atom on top of hollow, bridge and top sites. Here we found that the hollow site has the highest adsorption energy (1.37 eV), bridge site is quite close (1.28 eV) and top site has the lowest adsorption energy (0.91 eV). Compared to the case of gold on graphene, adsorption energies are much higher. And while on graphene Au preferred the top site, here it preferred the hollow site.

To illustrate the movement of the Au atom on 2D Au, we once again performed potential energy surface calculations, the results of which can be seen in Fig. 6a. Here the Au atom follows the path hollow-bridge-top-hollow. As can be seen, an Au atom moving on top of 2D Au would most likely hop between the hollow sites via bridge sites, with a 90 meV energy barrier. Compared to graphene, the energy barriers here are much higher, especially on the paths involving the top site.

D. Stage 4: Gold at the edge of 2D gold

In the final stage of the study, we investigated a gold atom at the edge of 2D gold patch, modeled by a 1D gold ribbon. Like with graphene, a 1D Au edge was constructed with 3-9 atomic rows, and the energy per atom was calculated and plotted with respect to the number of rows (Fig. 3a). The obtained edge energies are shown in Fig. 3b.

We studied the adsorption of a single Au atom on the edge, with two adsorption sites of interest: hollow site on top of the 1D Au, and an edge site on the side. The calculations were performed with 5 rows of Au atoms while the two bottom rows were fixed during the optimization.
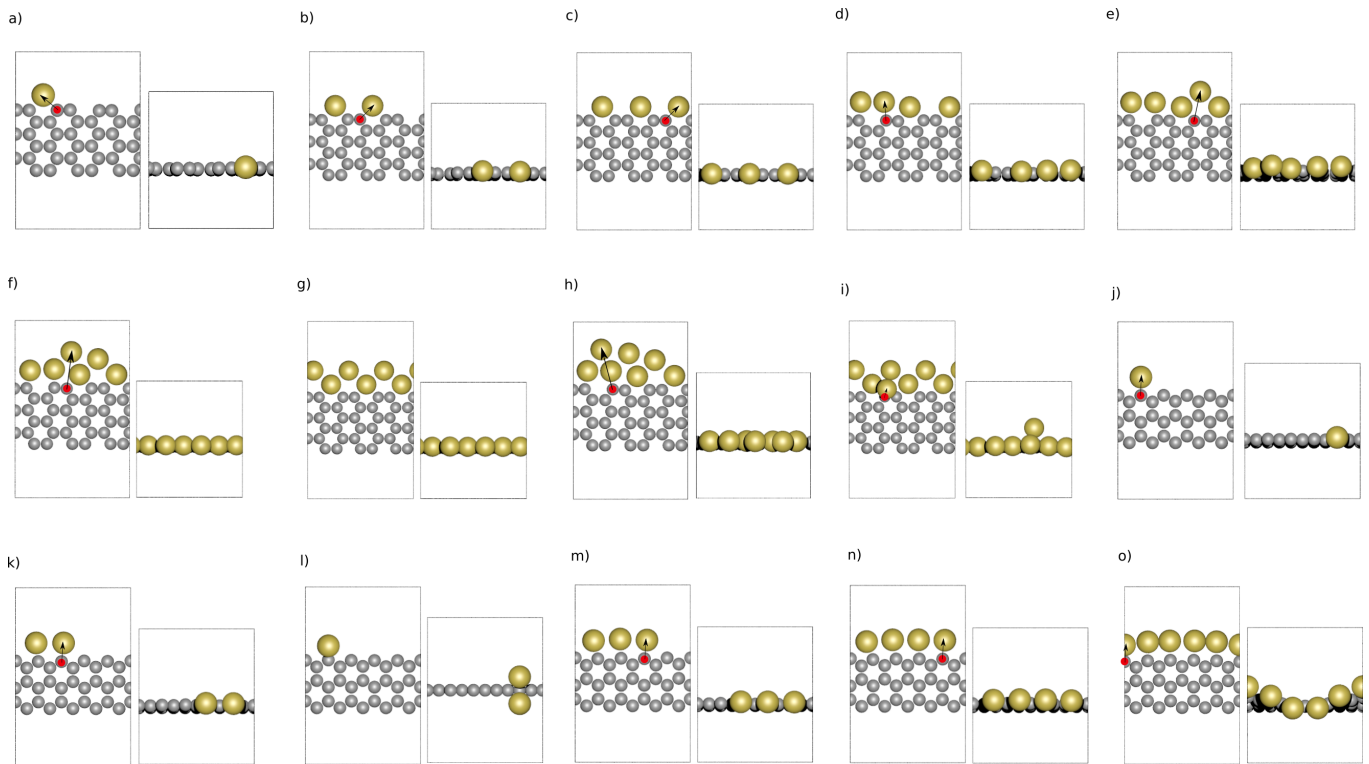
Fig. 5. Unit cells of AGNR and ZGNR systems with various amounts of gold at the edge, with a top view and a side view for each system. The red circle indicates the position in which the most recent Au atom was added (the atom that makes the growth), and the arrow points to the final position after optimization.
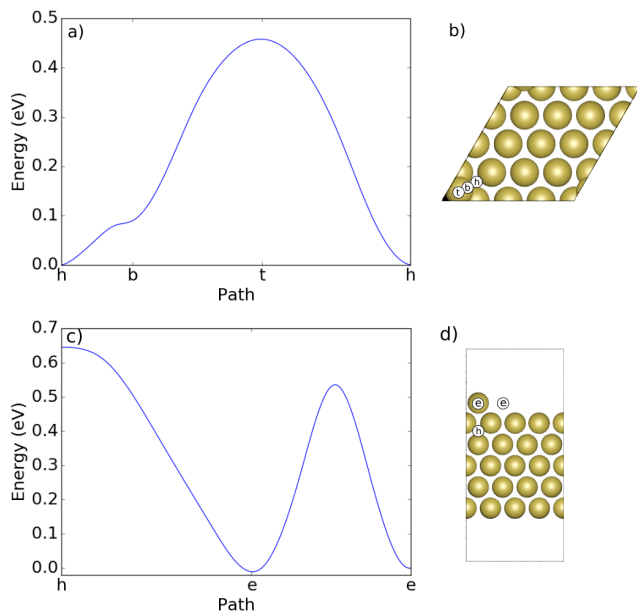

Fig. 6. a) PES of Au atom moving on top of 2D gold, b) the unit cell used in 2D gold calculations, with top [t], bridge [b] and hollow [h] sites marked, c) PES of Au atom moving near the 1D gold edge, and d) the unit cell used in 1D gold calculations, with hollow [h] and edge [e] sites marked.

As the result, the adsorption energy at the edge site (2.27 eV) was found to be considerably higher than at the hollow site (1.62 eV). It is notable that the optimization of an Au atom at a hollow site close to the edge brought the Au atom much closer to the edge, almost to a bridge site.

The movement of the Au atom was studied along two paths, along a path from the hollow site on top of the 1D Au to the edge site (h-e) and along a path between two edge sites (e-e). The results of the calculations are shown in Fig. 6c. The atom was found to hop from the top to the edge easily, because there was no energy barrier. The movement along the edge however came with an energy barrier of ∼0.55 eV.

IV.   DISCUSSION

The adsorption energies and the distances to the nearest neighboring atom of a single gold atom on various adsorption sites are summarized in Table I. On top of graphene gold shows weak adsorption, while at the edge of graphene gold shows strong adsorption. There is also another possible adsorption site between the edge sites of ZGNR, as seen in Fig. 4, although the energy barrier separating the sites is low (<10 meV), and our simulations suggest that the lower-energy edge sites are much more likely to get occupied by the incoming gold atoms.

The overall picture of the growth process is quite clear, at least when viewed via the potential energy surface.

Table I. Au atom adsorption energies E_{ads} (eV) and distances d (Å) to nearest atoms at different adsorption sites on graphene, 2D Au, AGNR, ZGNR and 1D Au.

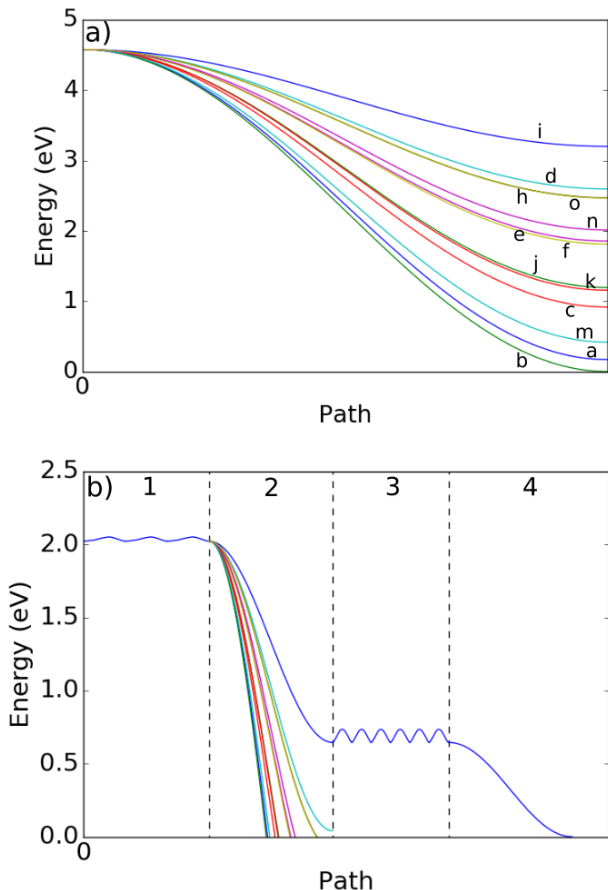|	hollow		bridge		top		edge	
	E_{ads}	d	E_{ads}	d	E_{ads}	d	E_{ads}	d
1 Graphene	0.073	3.57	0.096	3.19	0.102	3.08	-	-
2 AGNR	-	-	-	-	-	-	5.62	2.13
2 ZGNR	-	-	-	-	-	-	4.61	1.97
3 2D Au	1.37	2.81	1.28	2.75	0.91	2.67	-	-
4 1D Au	1.62	2.71	-	-	-	-	2.27	2.67

Fig. 7. a) PES of Au atom moving from the top of graphene to the edge with different number of gold atoms at the edge. Each graph represents a system as seen in Fig. 5. b) The overall PES for an Au atom contributing to the growth of the golden patch. Numbers 1-4 indicate the systems all pictured in Fig. 1, with number 2 more detailed in a. The blue path thus illustrates only one possible PES for a gold atom during the growth process.

Figure 7b illustrates the PES of gold atoms on their path to the edge. The extremely low energy barrier ($\sim$30 meV) shows that a gold atom is likely to move readily on top of graphene. Moreover, it continues to move from the top to the edge without an energy barrier. The same trend continues even when more gold atoms are added. Interestingly, there is also a possibility for the new gold atoms to replace old gold atoms in the first row and nudge them further to the second row. This would imply that patches grow not only at the edge, but also at the graphene-gold interface.

Furthermore, as with graphene, the energy barrier of a gold atom moving on top of 2D gold is very low (90 meV on hollow-bridge-hollow path), and no energy barrier was found when moving to the edge of 2D gold. While atoms move to the edge effortlessly, there still exists energy barriers when moving along the edge. The armchair edge has particularly large barrier when moving along the edge (1.7 eV). We note that the choice of exchange-correlation functional affects more on adsorption energies and less on diffusion energy barriers. Since our main interest here is on energy barriers, our choice to exclude vdW interactions should be a reasonable approximation, as demonstrated in the study of Amft et al.[22] Overall, the low energy barriers and the ease of the growth of the gold patch is not exactly surprising, but our study does further clarify the picture of the interaction of gold and graphene edge.

It is probable that higher temperature studies would trigger a collapse of the 2D gold patch into a 3D nanoparticle. Zhao et al. observed this kind of collapse for a 2D Fe patch when the Fe particles were under prolonged electron irradiation: they found that the Fe membrane-armchair graphene interface remained stable the longest, compared to Fe-zigzag graphene interface.[7] Nevertheless, the 2D Fe membranes remained stable for several minutes under the irradiation. The low energy barriers of our study (<0.5 eV) indicate that room temperature (300 K) should be enough for rapid diffusion and patch growth. It is expected that the effects of temperature are greatest in the stage 2 of our study, at the gold-graphene interface, as the potential energy drops are the highest for these systems, thus increasing the kinetic energy the most.

In summary, we have studied the growth of 2D gold patch at the graphene zigzag and armchair edges. We hope this study clarifies the microscopic processes during the growth of a 2D metal patch in graphene pores and encourages experiments to fabricate a stable 2D metal monolayer. As shown by this study, gold makes an excellent candidate for this because of its low diffusion barriers and strong binding with the graphene edge; experiments should be quite feasible in room temperature.

[1] Li-Ming Yang et al., *The New Dimension of Silver*, Phys. Chem. Chem. Phys., 2015, 17, 19695-19699

[2] Yuanbo Zhang et al., *Experimental observation of the*

quantum Hall effect and Berry's phase in graphene, Nature 438, 201-204

[3] Kin Fai Mak et al., *Atomically Thin MoS$_2$: A New Direct-Gap Semiconductor*, Phys. Rev. Lett. 105, 136805

[4] Andrea Splendiani et al., *Emerging Photoluminescence in Monolayer MoS$_2$*, Nano Lett., 2010, 10 (4), pp 12711275

[5] Li-Ming Yang, M. Dornfeld, T. Frauenheim, and E. Ganz, *Glitter in a 2D monolayer*, Phys. Chem. Chem. Phys., 2015, 17, 26036

[6] Pekka Koskinen and Topi Korhonen, *Plenty of Motion at the bottom: Atomically Thin Liquid Gold Membrane*, Nanoscale, 2015, 7, 10140

[7] Jiong Zhao et al., *Free-Standing Single-Atom-Thick Iron Membranes Suspended in Graphene Pores*, Science 343, 1228 (2014)

[8] Yangfan Shao et al., *Stability of Two-Dimensional Iron Carbides Suspended across Graphene Pores: First-Principles Particle Swarm Optimization*, J. Phys. Chem. C 2015, 119, 22954-22960

[9] A. Sanchez et al., *When Gold Is Not Noble: Nanoscale Gold Catalysts*, J. Phys. Chem. A 1999, 103, 9573-9578

[10] Mikael P. Johansson et al., *2D-3D transition of gold cluster anions resolved*, Phys. Rev. A 77, 1 (2008)

[11] Hannu Häkkinen et al., *Bonding in Cu, Ag, and Au Clusters: Relativistic Effects, Trends, and Surprises*, Phys. Rev. Lett. 89, 33401

[12] Hongtao Wang et al., *Interaction between single gold atom and the graphene edge: A study via aberration-corrected transmission electron microscopy*, Nanoscale, 2012, 4, 2920

[13] S. R. Bahn and K. W. Jacobsen, *An object-oriented scripting interface to a legacy electronic structure code*, Comput. Sci. Eng., Vol. 4, 56-66, 2002

[14] J. J. Mortensen, L. B. Hansen , and K. W. Jacobsen, *Real-space grid implementation of the projector augmented wave method*, Physical Review B, Vol. 71, 035109, 2005

[15] J. Enkovaara, C. Rostgaard, J. J. Mortensen et al. *Electronic structure calculations with GPAW: a real-space implementation of the projector augmented-wave method*, J. Phys.: Condens. Matter 22, 253202 (2010)

[16] P. E. Blöchl, *Projector augmented-wave method*, Physical Review B, Vol. 50, 17953, 1994

[17] J. P. Perdew, K. Burke, and M. Ernzerhof, *Generalized Gradient Approximation Made Simple*, Phys. Rev. Lett. 77, 3865 (1996)

[18] C. G. Broyden, *The convergence of a class of double rank minimization algorithms: 2. The new algorithm*, J. Inst. Math. Appl. 6, 222-231 (1970)

[19] G. Henkelman and H. Jonsson, *Improved Tangent Estimate in the NEB method for Finding Minimum Energy Paths and Saddle Points*, J. Chem. Phys. 113, 9978 (2000)

[20] M. Amft et al., *Small gold clusters on graphene, their mobility and clustering: a DFT study*, J. Phys.: Condens. Matter 23, 205301 (2011)

[21] Sami Malola et al., *Gold in graphene: In-plane adsorption and diffusion*, Appl. Phys. Lett. 94, 043106 (2009)

[22] M. Amft et al., *Adsorption of Cu, Ag, and Au atoms on graphene including van der Waals interactions*, J. Phys.: Condens. Matter 23 (2011) 395001

[23] Pekka Koskinen et al., *Self-Passivating Edge Reconstructions of Graphene*, Phys. Rev. Lett. 101, 115502 (2008)